Clin Transl Imaging (2013) 1:423–432
DOI 10.1007/s40336-013-0040-0

REVIEW ARTICLE

Multiagent imaging of liver tumors with reference to intra-arterial radioembolization

Marco Maccauro · Alice Lorenzoni · Giuseppe Boni · Carlo Chiesa · Carlo Spreafico · Raffaele Romito · Vincenzo Mazzaferro · Ettore Seregni

Received: 2 September 2013 / Accepted: 11 November 2013 / Published online: 3 December 2013

Abstract Intra-arterial radioembolization using microspheres labeled with the high-energy beta-emitter yttrium-90 (^{90}Y) is an innovative therapeutic strategy for primary and secondary hepatic malignancies. An accurate imaging workup plays a pivotal role in correctly selecting patients for treatment, to avoid severe complications and in assessment of the post-administration microsphere distribution. Nuclear medicine imaging modalities are an integral part of a complex multidisciplinary approach. In particular, hepatic perfusion imaging with ^{99m}Tc-macroaggregated albumin particles (^{99m}Tc-MAA), which identifies extrahepatic accumulation of radiopharmaceutical and lung shunt, is necessary to correctly select patients who may benefit from the treatment. Furthermore, ^{99m}Tc MAA SPECT-based dose planning may optimize RE efficacy, overcoming the limitations of empirical methods to determine the activity to be administered. Quantitative assessment of the post-administration intrahepatic microsphere distribution with SPECT or PET is important for evaluation of toxicity and efficacy and can be used for the prediction of patient response and for patient-specific therapeutic dose optimization. Finally, [^{18}F]FDG PET/CT imaging is important in the assessment of early response after RE and in predicting patient outcome. This review provides a comprehensive overview of multimodality imaging in the complex management of patients undergoing RE for liver tumors.

Keywords Intra-arterial radioembolization · ^{90}Y microspheres · ^{99m}Tc-MAA · ^{90}Y PET

Introduction

Primary liver cancer is the sixth most common cancer and the third cause of cancer-related death worldwide, responsible for 500,000 deaths per year [1]. Furthermore, the liver is the most common site of cancer metastases and up to 25 % of patients with malignancies will develop hepatic lesions, especially from colorectal, pancreatic and breast cancer. Fewer than 10 % of patients with hepatocellular carcinoma (HCC) or liver metastases are candidates for radical treatment, the majority being unsuitable due to advanced stage at presentation, presence of hepatic dysfunction or presence of co-morbidities. Local treatment, such as radiofrequency ablation or transarterial chemoembolization (TACE), and systemic therapy with cytotoxic drugs are alternative palliative treatments in patients with non-resectable disease.

Because of their characteristic blood supply, primarily from the hepatic artery, and their hypervascularization—they are up to three times more vascularized than normal parenchyma–liver lesions are suitable for loco-regional therapy by intra-arterial administration of drugs. Several

Color figures online at http://link.springer.com/article/10.1007/s40336-013-0040-0.

M. Maccauro (✉) · A. Lorenzoni · C. Chiesa · E. Seregni
Nuclear Medicine Division, National Cancer Institute, Milan, Italy
e-mail: marco.maccauro@istitutotumori.mi.it

G. Boni
Regional Center of Nuclear Medicine, University of Pisa, Pisa, Italy

C. Spreafico
Department of Radiology, National Cancer Institute, Milan, Italy

R. Romito · V. Mazzaferro
Departments of Surgery, Liver Transplantation and Gastroenterology, National Cancer Institute, Milan, Italy

techniques have been developed to selectively target liver tumors; these include administration of cytostatic drugs or intra-arterial embolization techniques. Intra-arterial radioembolization (RE) using microspheres labeled with the high-energy beta-emitter yttrium-90 (^{90}Y) is an innovative local therapy for conditions in which, to date, systemic therapy was the only option [2]. This procedure allows the tumor to be irradiated with a dose higher than that allowed by whole-liver external beam radiation treatment, in which doses are limited to 30–40 Gray (Gy). Radioembolization with ^{131}I-lipiodol has been used in patients with HCC as an adjuvant therapy, showing good results compared with chemoembolization even in patients with portal vein thrombosis, although without any survival advantage [3]. The retention of radiolabeled lipiodol in HCC after intra-arterial infusion is related to embolization in the tumor microvessels and to its entry into the interstitium and into neoplastic cells and it shows an inverse relationship with tumor size. Several clinical studies have shown that treatment with ^{131}I-lipiodol is well tolerated and only rare cases of neutropenia and thrombocytopenia have been observed [4–7]. Lipiodol has also been conjugated with renium-188 (^{188}Re) for the treatment of HCC and similar biodistribution data have been reported. Two phase II studies dealing with the treatment of advanced HCC showed that ^{188}Re-lipiodol treatment is feasible and well tolerated [8, 9]. Nowadays, selective internal radiation therapy (SIRT) performed with microspheres labeled with the high-energy beta-emitter ^{90}Y is increasingly being used for the treatment of patients with non-resectable primary or metastatic liver tumors. It can be performed by injection of the radiopharmaceutical into the proper hepatic artery or into the right (RHA) and left hepatic arteries (LHA) separately in the same session (whole-liver treatment), or into the RHA and LHA sequentially with a 4-week interval between the two injections (lobar treatment). Whole-liver treatment should be avoided in cases of HCC and carefully evaluated for the treatment of metastatic lesions; however, treatments should be as selective as possible to optimize efficacy and reduce side effects.

Yttrium-90 microspheres

In the 1960s, Blanchard et al. [10] explored the concept of intra-arterial RE by injecting ^{90}Y-containing microspheres into the hepatic artery of tumor-bearing rabbits. The favorable results of ^{90}Y-microsphere RE treatment in different animal models led to the clinical development of this technique in the 1970s. The first clinical investigations [11–14] were conducted in the 1980s in selected patients and they gave encouraging results. However, the release of free isotope into the circulation due to leaking of ^{90}Y from the microspheres caused severe pancytopenia in several patients. In order to overcome the problem of degradation of the bond between ^{90}Y and the microspheres, new radiopharmaceuticals were developed. Two microsphere products are available commercially: one (Thera-Sphere® MDS Nordion, Canada) consists of glass microspheres containing native, non-radioactive yttrium-89 (which is then converted ^{90}Y by neutron irradiation), characterized by a mean diameter of 25 ± 1 μm and high specific activity (2,500 Bq per sphere). In this case, the in vitro release of ^{90}Y is less than 0.13 % after 6 weeks of incubation in saline solution. The other commercially available product consists of ^{90}Y resin microspheres (SIR-Spheres® SirTex Ltd, Australia), characterized by a mean diameter of 32 ± 10 μm and a lower specific activity (50 Bq per sphere). Labeling of these microspheres with ^{90}Y is based on cation exchange, a reversible process in isotonic solution. In this case, stability studies showed that the release of ^{90}Y is <0.4 % in water after 20 min of incubation and the levels in blood and urine of treated patients are inferior to 50 KBq/L. The standard activity per vial is 3 GBq, corresponding to 1.2 and 40–80 million microspheres for the glass-based and resin-based products, respectively. The embolic effect of resin microspheres could result in a therapeutic advantage due to the related ischemia, but also in side effects such as pain, fever and nausea, especially in patients with cirrhosis.

Imaging work-up prior to SIRT

The incidence of gastrointestinal complications following RE has been found to range from 3 to 5 % [15], sometimes exceeding 10 %. The major causes of gastroduodenal ulcers are the extrahepatic infusion of radiolabeled microparticles through arteries originating from the hepatic arterial branches and microsphere reflux occurring during the injection. An accurate imaging workup prior to ^{90}Y-microsphere administration is a crucial part of the therapeutic management of patients undergoing RE to correctly select those who may benefit from the therapy. An angiographic evaluation of the visceral arteries prior to RE should also be performed to evaluate anatomical variants and extrahepatic arteries feeding the tumor. Moreover, ^{99m}Tc-MAA scintigraphy plays a pivotal role in identifying gastroduodenal accumulation and lung shunt.

Angiographic evaluation

To establish the vessel anatomy, abdominal aortography followed by selective visceral angiography is performed. Furthermore, superior mesenteric arteriography should also

Fig. 1 Phrenic artery embolization (*white arrow*) during angiographic study

be performed to evaluate the presence of accessory or replaced hepatic arteries. The status of the portal vein may be assessed with angiograms acquired during the venous phase, even though this information can be obtained with CT/MRI. Selective right and left hepatic angiography allows identification of any variant mesenteric anatomy and subsequent prophylactic embolization of extrahepatic vessels such as the right gastric, gastroduodenal or falciform artery. Normal celiac trunk anatomy is present in only 55 % of patients. In these cases the proper hepatic artery originates from the common hepatic artery, which also gives rise to the gastroduodenal artery. The proper hepatic artery continues as the right hepatic artery, giving off the left hepatic artery. The most common anatomical variants, occurring in 10 % of cases, consist of a left hepatic artery originating from the left gastric artery or a right replaced hepatic artery originating from the superior mesenteric artery. In about 8 % of cases, an accessory right (7 %) and left (8 %) hepatic artery may originate, respectively, from the left gastric and the superior mesenteric artery [16]. The extrahepatic vessels originating from the hepatic arteries have to be occluded in order to isolate the hepatic circulation (Fig. 1) [17, 18]. The largest extrahepatic vessel, originating from a hepatic artery, is the gastroduodenal artery. The next most important extrahepatic vessel is the right gastric artery, most often originating from the proper or left hepatic artery. The falciform artery is a less common extrahepatic artery, but failure to identify and embolize it may cause severe complications such as abdominal pain, peri-umbilical skin rash and skin necrosis. Other vessels that may be identified and may require prophylactic embolization include the supraduodenal, retroduodenal, left inferior phrenic, accessory left gastric and inferior esophageal arteries. A detailed evaluation during angiography should be performed to make certain that hepatic arteries do not originate from an extrahepatic vessel. In fact the anatomy of the gastroduodenal artery should be carefully explored and embolization avoided if it is found to supply the hepatic parenchyma. Prophylactic embolization of the cystic artery is a controversial practice because it may lead to ischemic cholecystitis [19]. Furthermore, the gallbladder may also be supplied by collaterals or perforators from the hepatic parenchyma and the incidence of radiation-induced cholecystitis is very low. It may be difficult to establish whether a vessel is a hepatic or extrahepatic branch or a combination. In such cases, computed tomography (CT) angiography with intravenous or intra-arterial contrast-injection may help to identify the correct anatomy [20].

Hepatic perfusion imaging

Liver perfusion imaging with ^{99m}Tc-MAA, serving to identify sites of non-targeted distribution of the radiopharmaceutical or the presence of lung shunt, is an indispensable step before RE with ^{90}Y-microspheres. The radiotracer is injected during angiography (185 MBq) into the branch of the hepatic artery supplying the target volume to simulate the treatment with ^{90}Y-microspheres. If the whole liver is being evaluated for treatment, the usual dose injected into the right and left hemi-liver is approximately 111 MBq (3 mCi) and 74 MBq (2 mCi), respectively. The ^{99m}Tc-MAA used in pretreatment investigative perfusion studies are 30–90 nm in diameter, similar in range but not identical in size and shape to ^{90}Y-microspheres. Anterior and posterior planar images of the whole body are obtained within 1 h of MAA injection to calculate the fraction of ^{99m}Tc-MAA shunted to the lungs (Fig. 2) and to detect any extrahepatic accumulation of radiopharmaceutical. The limit of injected activity shunted to the lungs with TheraSpheres is 610 MBq/mL [21]. As regards SIR-Spheres, the proposed activity for the treatment should be adjusted to the percentage of hepatopolmunary lung shunting, and in the presence of a value superior to 20 %, administration of SIR-Spheres is contraindicated [22]. These limitations are applied to avoid exceeding a maximum radiation dose of 30 Gy to the lungs [23]. In a study performed by Rose and colleagues [24], chemoembolization with acrylated collagen reduced the lung shunt, permitting a subsequent ^{90}Y therapy. Bester et al. [25] instead proposed temporary occlusion of shunts through the endovascular placement of balloon catheters in the hepatic veins. However, neither technique has yet been validated for safety and efficacy. The in vivo biodegradation of ^{99m}Tc-MAA in the liver and the presence of free ^{99m}Tc-pertechnetate in the systemic

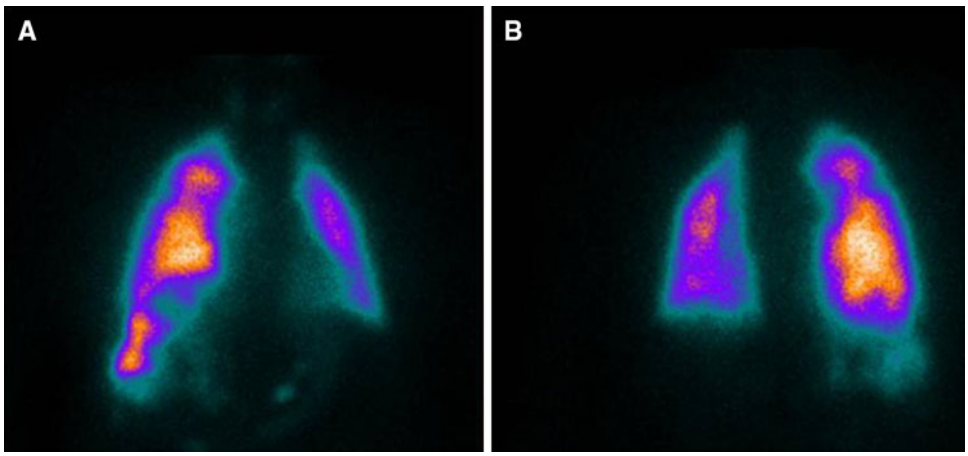

Fig. 2 Hepatic perfusion study planar image (**a** *anterior view*; **b** *posterior view*) demonstrating severe lung shunt (a contraindication to the treatment) (color figure online)

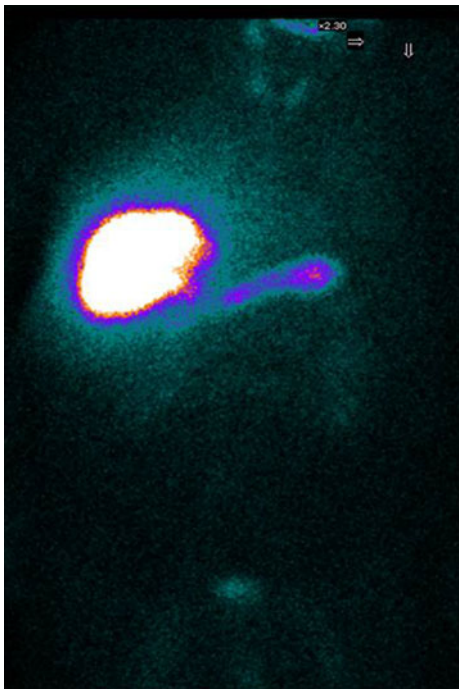

Fig. 3 Whole-body study (*anterior view*) in a patient submitted to ^{99m}Tc-MAA scintigraphy revealing the presence of activity in the thyroid gland, kidneys and stomach due to free ^{99m}Tc-pertechnetate (color figure online)

circulation should be correctly evaluated. In this latter circumstance scintigraphy will reveal the presence of activity in the thyroid gland, kidneys and stomach (Fig. 3). A delay in image acquisition after the angiographic procedure may result in significant in vivo degradation of the radiopharmaceutical with high background activity and should, therefore, be avoided. Any activity visualized in the stomach should be carefully evaluated to distinguish between free ^{99m}Tc-pertechnetate (which characteristically involves the entire gastric mucosa as well as the thyroid gland) and extrahepatic perfusion, which is imaged as a focal area of accumulation in the stomach wall. The administration of perchlorate before angiography prevents non-specific uptake of ^{99m}Tc-pertechnetate in the thyroid and stomach. The extrahepatic sites of ^{99m}Tc-MAA accumulation are unlikely to be detectable on planar images because of the low spatial resolution; thus SPECT of the abdomen should be performed to avoid severe complications after SIRT (Fig. 4). Careful analysis of tomographic images is important to accurately distinguish whether the ^{99m}Tc-MAA has accumulated in the liver or in adjacent organs (Fig. 5). SPECT/CT more accurately identifies sites of extrahepatic activity than does SPECT or planar imaging only. Ahmadzadehfar and colleagues [26] reported that extrahepatic accumulation was detected by planar imaging, SPECT and SPECT/CT in 12, 17 and 42 % of examinations, respectively. The SPECT/CT findings affected management in 29 % of patients. The sensitivities were 100, 41 and 32 % and the specificities 98, 98 and 93 % for SPECT/CT, SPECT and planar imaging, respectively. In a prospective study Hamami et al. [27], evaluating 68 ^{99m}Tc-MAA procedures performed in 58 patients with HCC, demonstrated a superior performance of SPECT/CT over SPECT and planar imaging (sensitivity 100 %, specificity 94 % for SPECT/CT versus 56 and 87 %, respectively, for SPECT). Similarly, in a report published by Lenoir et al. [28] the superiority of SPECT/CT over planar imaging was demonstrated analyzing 136 hepatic perfusion scintigraphies. In ~36 % of the cases SPECT/CT had a potential impact on patient management. In a study by Dudeck et al. [29] on repeated angiography in patients designated for ^{90}Y RE in the event of extrahepatic ^{99m}TcMAA accumulation, gastroduodenal uptake was identified in 33 patients (9.7 %) using SPECT/CT. During the subsequent angiography procedure the gastroduodenal shunt was correctly identified and corrected in 31 out of the 33 patients. A discrepancy between the distribution of ^{99m}Tc-MAA in the liver and the vascular territory to be treated may occur in a small percentage (<4 %) of cases and can be explained by different injection rates and different arterial flow between soluble

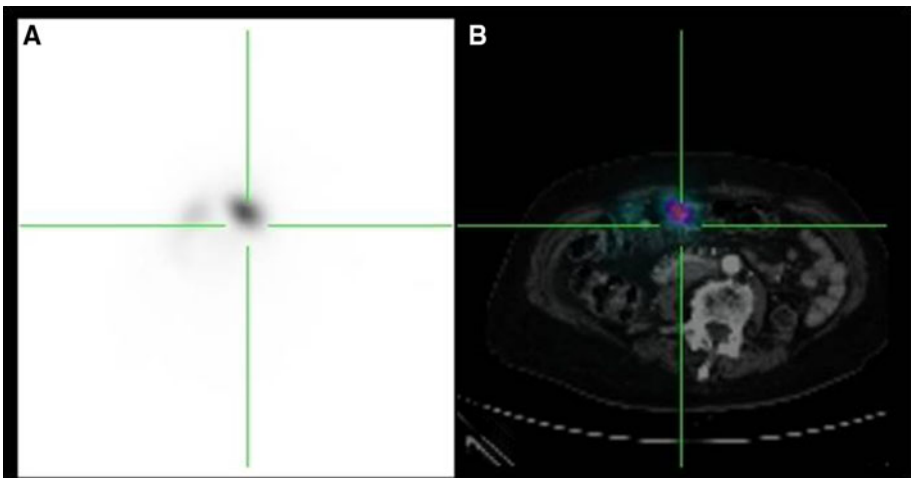

Fig. 4 SPECT/CT image of the abdomen (**a** SPECT *axial view*, **b** *axial fused image*) demonstrating intestinal accumulation of ^{99m}Tc-MAA (color figure online)

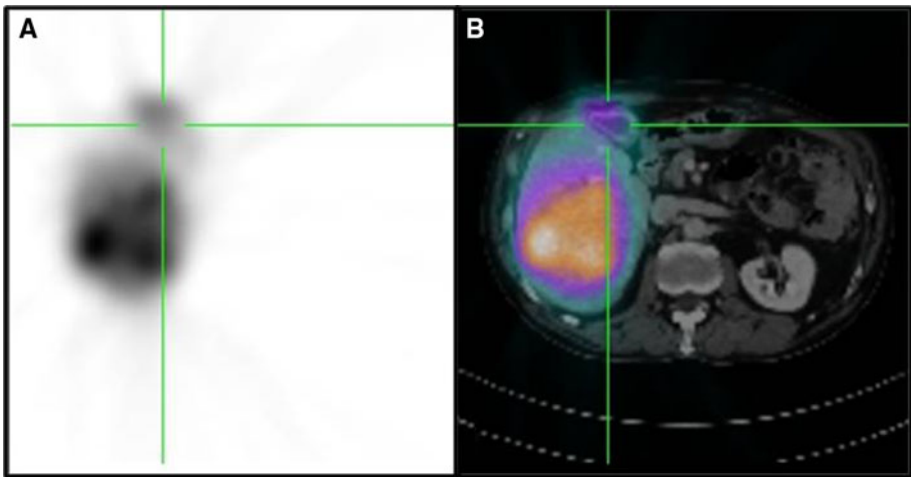

Fig. 5 SPECT/CT image of the abdomen (**a** SPECT *axial view*, **b** *axial fused image*) showing the presence of extrahepatic accumulation in the gallbladder after ^{99m}Tc-MAA injection (color figure online)

contrast molecules versus ^{99m}Tc-MAA, or to different locations of the microcatheter tip between the diagnostic phase and the treatment phase. Kao and colleagues [30] showed that ^{99m}Tc-MAA SPECT/CT more accurately represents hepatic microparticle biodistribution than does soluble contrast hepatic angiography. Alternatively, the tumor may have an unidentified accessory arterial blood supply or may have caused vascular remodeling of the local arteries. This possibility is more common in patients previously submitted to TACE treatment of the primary tumor-supplying arteries. SPECT/CT plays a pivotal role in treatment planning, making it possible to determine liver volume and dosimetry prior to injecting radiolabeled ^{90}Y-microspheres.

Treatment planning with ^{99m}Tc-MAA SPECT

The methods most commonly used to determine the activity of ^{90}Y-microspheres to be administered (delivered absorbed dose of 120 ± 20 Gy in the injected region for glass particles and BSA method for resin particles) should be replaced by the evaluation of tumor and non-tumor individual absorbed dose. The relationship between the ^{99m}Tc-MAA SPECT-based tumor absorbed dose and tumor response is reported in several studies investigating the possibilities of treatment optimization by individualized ^{99m}Tc-MAA SPECT-based dose planning. All published studies found a dose-efficacy correlation: with resin spheres, both in HCC [31] and in CRC metastases [32, 33], and with glass spheres in HCC [34, 35]. Statistically significant differences in the most important oncological end points, i.e., overall survival, progression-free survival and time to progression, were correlated with lesion absorbed doses higher or lower than about 200 Gy with glass spheres in HCC [36, 37]. As regards radio-induced liver toxicity, Sangro et al. [38] found that the threshold for RE-induced liver disease (REILD) with resin spheres is an activity greater than 0.8 GBq/L, which corresponds to 50 Gy kg/GBq × 0.8 GBq/1 kg = 40 Gy mean absorbed dose to non-tumoral parenchyma. On multivariate analysis repeated on the subset of REILD patients, young age and mean

absorbed dose to non-tumoral parenchyma emerged as independent risk factors. Chiesa et al. [39] found the first dose-toxicity correlation for glass spheres, the limit of 70 Gy averaged on the whole non-tumoral parenchyma being found to keep liver failure risk below 20 %. The difference in the healthy liver dose limit for the two kinds of spheres seems attributable to the different number of particles and consequent differences in non-uniformity of dose distribution at the microscopic level.

Methodologically, because of permanent trapping of microspheres (absence of biological clearance), SPECT imaging can be acquired at any time after administration. Simple patient-specific quantification is based on the counts-to-activity calibration factor obtained as the total injectable ^{90}Y-microsphere activity divided by total counts in the ^{99m}Tc-MAA SPECT field of view. Absorbed dose D is computed using the well-known approximation of the MIRD formalism: D[Gy] = 50 A[GBq]/M[kg], where A is the activity in a region, determined through counts in a ROI defined over that region and the calibration factor, and M is its mass, measured on SPECT and/or CT. The only requirement for this methodology is an attenuation-corrected ^{99m}Tc-MAA SPECT study, which is intrinsically provided by a hybrid SPECT/CT single gantry [40].

A limitation of pre-treatment dosimetry is the possible mismatch between ^{99m}Tc-MAA and ^{90}Y-microsphere biodistributions. This may arise not only from an intentionally or inadvertently different catheter position, but also from intrinsic differences in the number of particles. The number of albumin particles is significantly lower than the number of injected ^{90}Y-microspheres (0.1–0.2 millions of MAA versus 30–60 millions of resin and 4–5 millions of glass particles), and a similar pattern is seen with the density (1.1 versus 1.6 g/mL for resin and 3.3 g/mL for glass particles). These features might explain why the mismatch problem seems to be more serious for embolic resin spheres [41–43]. The literature is controversial, however, since Kao et al. [44], for instance, found excellent correspondence between ^{99m}Tc-MAA SPECT and ^{90}Y PET dosimetry (median relative error 3.8 %).

Post-treatment imaging workup

Quantitative assessment of post-administration intrahepatic microsphere distribution is important for evaluation of RE toxicity and efficacy and can potentially be used for the prediction of patient response and patient-specific therapeutic dose optimization. Considering the mainly beta emission of the radionuclide, the in vivo imaging of ^{90}Y to determine tumor targeting and to perform dosimetric studies is challenging. Furthermore, the biodistribution of ^{99m}Tc-MAA may imperfectly predict that of ^{90}Y-labeled microspheres. The possibilities for imaging distribution of ^{90}Y-microspheres include SPECT acquisition using the bremsstrahlung emission and PET/CT using the transition of ^{90}Y to zirconium-90. Although bremsstrahlung imaging of ^{90}Y is widely used in clinical practice, in the absence of a photopeak, SPECT imaging is dependent on the continuous bremsstrahlung X-rays; this results in low spatial resolution and poor quantification performance. The absence of a photopeak prohibits the use of simple window-based scatter rejection, scatter correction, and attenuation correction techniques, and penetration of high-energy photons through the collimator septa leads to further loss of image contras. Several reconstruction algorithms and imaging protocols have been proposed to overcome these technical limitations [41, 45]. The use of pinhole collimators seems to result in better contrast recovery coefficients compared with those obtained with parallel-hole collimators. The different designs and the attenuating material used for the collimation may explain these data [46]. Ahmadzadehfar et al. [47] evaluated the significance of post-therapy bremsstrahlung SPECT/CT images in the prediction of RE-induced extrahepatic side effects in 188 procedures. The results showed that detection of extrahepatic activity on bremsstrahlung SPECT/CT scans predicted gastrointestinal ulcers with a sensitivity of 87 % and a specificity of 100 %, despite low image quality. The positron emission of ^{90}Y (32 positrons per second per MBq) with a maximum energy of 758 keV is suitable for PET imaging, allowing the detection of extrahepatic activity and accurate tumor and liver dose estimation. Moreover, the correction techniques for scatter, random, and attenuation effects that are clinically available for ^{18}F PET can be directly applied to ^{90}Y PET. Carlier and colleagues [48] demonstrated that the minimum radioactive concentration of ^{90}Y detectable by PET imaging is 1 MBq/mL. An activity concentration below 1 MBq/mL may also be detected, but with a variable quantitative accuracy depending on the lesion size and reconstruction parameters. The benefit of time-of-flight reconstruction has been shown particularly for concentrations below 2 MBq/mL or small lesion sizes. Evaluation of ^{90}Y-particle accumulation with PET/CT demonstrates high spatial resolution and low scatter compared with bremsstrahlung SPECT/CT (Fig. 6). Elschot and colleagues [49] showed that the image quality of PET is superior to bremsstrahlung SPECT for the assessment of ^{90}Y-microsphere distribution after RE. PET showed higher contrast recovery coefficients than SPECT. PET-based dose estimates were more accurate than SPECT-based dose estimates, with underestimations ranging from 45 to 11 % for PET, and 75 to 58 % for SPECT, respectively. Padia et al. [50] demonstrated that PET/CT shows spatial resolution at least comparable to that of ^{99m}Tc-MAA SPECT/CT in patients with large (>5 cm)

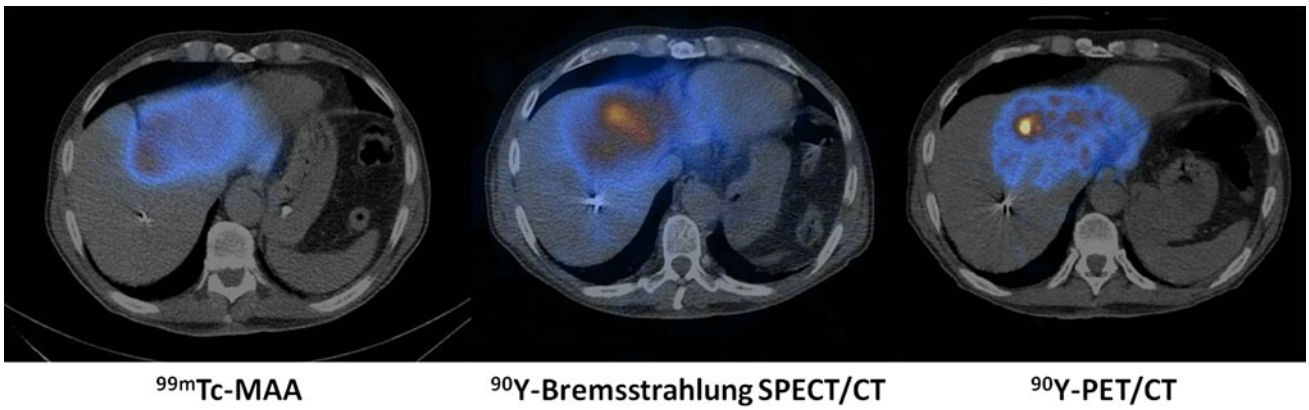

Fig. 6 Pretreatment ^{99m}Tc-MAA scintigraphy and post-treatment SPECT/CT and PET/CT of ^{90}Y microspheres show comparable biodistribution (color figure online)

HCC. Quantitative uptake in non-treated regions of interest showed significantly reduced scatter with PET/CT versus SPECT/CT (1 versus 14 %). The in vivo biodistribution of holmium microspheres may be studied with nuclear medicine imaging or MRI. In a study performed by Turner et al. [51] a tracer activity of ^{166}Ho-microspheres was administered in pigs to predict the total administered activity required to deliver a prescribed radiation absorbed dose to the liver (25 Gy). ^{166}Ho-PLLA-MS SPECT imaging was found to be useful for quantitative analysis and for correctly calculating the absorbed dose. The pretreatment scout dose may be helpful for adjusting the delivered activity and the treatment dose distribution can be evaluated in a similar way. Finally, ^{166}Ho-microspheres could also be administered under real-time MRI guidance, with direct visualization of the microsphere distribution. Post-administration intrahepatic microsphere distribution was first evaluated with MRI in phantom and animal models by Nijsen and colleagues [52], who showed that Ho-PLLA-MS can be imaged clearly in vivo with MRI. Estimation of the absorbed radiation dose with MRI was performed in 15 patients submitted to whole-liver treatment (20–80 Gy). SPECT images were also acquired 3–6 days after administration of Ho-PLLA-MS. The mean whole-liver absorbed radiation dose calculated on MRI correlated with the absorbed radiation dose on SPECT and a more detailed intra-tumor biodistribution assessment was possible due to the better spatial resolution of MRI.

The role of [^{18}F]FDG PET/CT in SIRT

The criteria for assessing response following ^{90}Y RE are various and include standard size criteria as well as the presence of necrosis, angiographic avascularity and increased water diffusion on diffusion-weighted MRI. Paradoxical increases in size due to acute tumor necrosis are frequent; thus, post-RE morphological changes on early follow-up can make it difficult to interpret cross-sectional images and evaluate treatment response. The development of functional imaging techniques including diffusion-weighted MRI and PET allows for early assessment of treatment response and even prediction of overall tumor response to intra-arterial therapies. The utility of [^{18}F]FDG PET/CT for assessing tumor response in patients with primary or secondary hepatic malignancies undergoing intra-arterial therapies has been investigated. The metabolic information obtained from [^{18}F]FDG PET/CT in cases of [^{18}F]FDG-avid tumors seems to provide a more accurate and earlier assessment of therapy response following ^{90}Y-microsphere treatment than the morphological criteria measured on CT or MRI.

Wong and colleagues [53] investigated the role of [^{18}F]FDG PET in assessing treatment response in 19 patients with hepatic metastases from various solid tumors. The percentage decrease of total liver standardized uptake values (SUV) after treatment in the response group (−19 %) was significantly greater than that in the non-response group. Bienert et al. [54] evaluated tumor area, measured on CT, of 30 liver metastases and [^{18}F]FDG uptake to quantitatively assess changes in SUV and tumor size following ^{90}Y-microsphere treatment. A 20 % decrease in SUV from baseline at the follow-up PET/CT 1 month after treatment was taken as the response threshold. A wide range of post-treatment changes in target lesions was observed on CT, including an increase in the size of hypodense lesions, necrotic features and complete resolution of CT abnormalities. The changes in tumor size did not correlate with changes in [^{18}F]FDG uptake. [^{18}F]FDG PET imaging was found to be more sensitive than CT in the assessment of early response in a study performed by Szyszko et al. [55]. Eighty-six percent of patients showed decreased PET activity at 6 weeks while only 13 % showed a partial response in the size of tumor

on CT scan. Assessment of early responses with [^{18}F]FDG PET/CT has been found to be superior to assessment based on the RECIST criteria and changes in tumor density evaluated with CT. Furthermore, PET is the strongest predictor of progression-free survival in patients with liver metastases, demonstrating a correlation with tumor markers [56–58].

Future perspectives

Holmium poly(L-lactic acid) (PLLA) microspheres (Ho-PLLA-MS) containing neutron-activable ^{165}Ho were proposed as suitable candidates for RE treatment of hepatic malignancies in the early 1990s by Mumper and colleagues [59]. Holmium-l66 (^{166} Ho) is a beta (E_{max} 1.84 MeV, half-life of 27 h) and gamma emitter (81 keV) with a maximum soft-tissue range of 8.4 mm suitable for imaging with a gamma camera. The absorbed radiation dose per Bq of ^{166}Ho is lower than that of ^{90}Y (8.7 versus 28 mGy/MBq) due to their different physical characteristics. Nijsen et al. [60, 61] developed ^{166}Ho-PLLA-MS with a higher content of holmium (17 versus 9 %) and showed elevated retention in liver tumor (>95 %) in an animal model. The PLA microspheres, which have a mean diameter of 30 μm (range 20–50 μm), are biodegradable and result in no permanent liver embolization. Holmium is highly paramagnetic and can consequently be visualized by MRI. A recent phase I dose escalation study evaluated the safety and the maximum tolerated radiation dose (MTRD) of ^{166}Ho RE in 15 patients with liver metastases. The MTRD was identified as 60 Gy. Stable disease or partial response was achieved in 14 out of 15 patients at 6 weeks and in nine out of 14 patients (64, 95 % CI 39–84) at 12 weeks after SIRT [62].

Conclusion

Intra-arterial RE using microspheres labeled with the high-energy beta-emitter ^{90}Y is a promising therapy for primary and secondary liver tumors. The process of selecting patients to be treated involves several imaging techniques and is designed to optimize the clinical benefits and to avoid severe hepatic and extrahepatic complications. A pivotal role in the workup of these patients is played by nuclear imaging modalities, from ^{99m}TC-MAA for the evaluation of hepatic perfusion to [^{18}F]FDG PET for the assessment of response. Nuclear medicine also plays a crucial role in the evaluation of tumor and non-tumor individual absorbed dose, allowing treatment optimization through individualized dose planning and the relative correlation with patient outcome.

Conflict of interest Marco Maccauro, Alice Lorenzoni, Giuseppe Boni, Carlo Chiesa, Carlo Spreafico, Raffaele Romito, Vincenzo Mazzaferro, Ettore Seregni declare no conflict of interest.

Human and Animal Studies This article does not contain any studies with human or animal subjects performed by any of the authors.

References

1. Parkin DM, Bray F, Ferlay J, Pisani P (2005) Global cancer statistics, 2002. CA Cancer J Clin 55:74–108
2. Giammarile F, Bodei L, Chiesa C, Flux G, Forrer F, Kraeber-Bodere F, Brans B, Lambert B, Konijnenberg M, Borson-Chazot F, Tennvall J, Luster M, Therapy, Oncology and Dosimetry Committees (2011) EANM procedure guideline for the treatment of liver cancer and liver metastases with intra-arterial radioactive compounds. Eur J Nucl Med Mol Imaging 38:1393–1406
3. Raoul JL, Guyader D, Bretagne JF, Heautot JF, Duvauferrier R, Bourguet P, Bekhechi D, Deugnier YM, Gosselin M (1997) Prospective randomized trial of chemoembolization versus intra-arterial injection of ^{131}I-labeled-iodized oil in the treatment of hepatocellular carcinoma. Hepatology 26:1156–1161
4. Risse JH, Pauleit D, Palmedo H, Bender H, Bucerius J, Ezziddin S, Klein V, Grünwald F, Biersack HJ, Reichmann K (2007) Therapy of hepatocellular carcinoma with ^{131}I-lipiodol: patient dosimetry. Nuklearmedizin 46:192–197
5. Raoul JL, Guyader D, Bretagne JF, Duvauferrier R, Bourguet P, Bekhechi D, Deugnier YM, Gosselin M (1994) Randomized controlled trial for hepatocellular carcinoma with portal vein thrombosis: intra-arterial iodine-131-iodized oil versus medical support. J Nucl Med 35:1782–1787
6. Raoul JL, Duvauferrier R, Bretagne JF, Bourguet P, Heresbach D, Siproudhis L, Gosselin M (1993) Usefulness of hepatic artery injection of iodized oil and ^{131}I-labeled iodized oil before the therapeutic decision in hepatocellular carcinoma. Scand J Gastroenterol 28:217–223
7. Lau WY, Lai EC, Leung TW, Yu SC (2008) Adjuvant intra-arterial iodine-131-labeled lipiodol for resectable hepatocellular carcinoma: a prospective randomized trial-update on 5- and 10-year survival. Ann Surg 247:43–48
8. Bernal P, Raoul JL, Vidmar G, Sereegotov E, Sundram FX, Kumar A, Jeong JM, Pusuwan P, Divgi C, Zanzonico P, Stare J, Buscombe J, Minh CT, Saw MM, Chen S, Ogbac R, Padhy AK (2007) Intra-arterial rhenium-188 lipiodol in the treatment of inoperable hepatocellular carcinoma: results of an IAEA-sponsored multination study. Int J Radiat Oncol Biol Phys 69:1448–1455
9. Kumar A, Srivastava DN, Chau TT, Long HD, Bal C, Chandra P, le Chien T, Hoa NV, Thulkar S, Sharma S, le Tam H, Xuan TQ, Canh NX, Pant GS, Bandopadhyaya GP (2007) Inoperable hepatocellular carcinoma: transarterial 188Re HDD-labeled iodized oil for treatment-prospective multicenter clinical trial. Radiology 243:509–519
10. Blanchard RJ, Grotenhuis I, Lafave JW, Frye CW, Perry JF Jr (1964) Treatment of experimental tumors; utilization of radioactive microspheres. Arch Surg 89:406–410
11. Herba MJ, Illescas FF, Thirlwell MP, Boos GJ, Rosenthall L, Atri M, Bret PM (1988) Hepatic malignancies: improved treatment with intraarterial Y-90. Radiology 169:311–314
12. Mantravadi RV, Spigos DG, Tan WS, Felix EL (1982) Intraarterial yttrium 90 in the treatment of hepatic malignancy. Radiology 142:783–786

13. Houle S, Yip TK, Shepherd FA, Rotstein LE, Sniderman KW, Theis E, Cawthorn RH, Richmond-Cox K (1989) Hepatocellular carcinoma: pilot trial of treatment with Y-90 microspheres. Radiology 172:857–860
14. Ehrhardt GJ, Day DE (1987) Therapeutic use of ^{90}Y microspheres. Int J Rad Appl Instrum B 14:233–242
15. Naymagon S, Warner RR, Patel K, Harpaz N, Machac J, Weintraub JL, Kim MK (2010) Gastroduodenal ulceration associated with radioembolization for the treatment of hepatic tumors: an institutional experience and review of the literature. Dig Dis Sci 55:2450–2458
16. Michels NA (1953) Variational anatomy of the hepatic, cystic, and retroduodenal arteries; a statistical analysis of their origin, distribution, and relations to the biliary ducts in two hundred bodies. AMA Arch Surg 66:20–34
17. Maleux G, Heye S, Vaninbroukx J, Deroose C (2010) Angiographic considerations in patients undergoing liver-directed radioembolization with 90Y microspheres. Acta Gastroenterol Belg 73:489–496
18. Lewandowski RJ, Sato KT, Atassi B, Ryu RK, Nemcek AA Jr, Kulik L, Geschwind JF, Murthy R, Rilling W, Liu D, Bester L, Bilbao JI, Kennedy AS, Omary RA, Salem R (2007) Radioembolization with ^{90}Y microspheres: angiographic and technical considerations. Cardiovasc Intervent Radiol 30:571–592
19. Salem R, Lewandowski RJ, Sato KT, Atassi B, Ryu RK, Ibrahim S, Nemcek AA Jr, Omary RA, Madoff DC, Murthy R (2007) Technical aspects of radioembolization with ^{90}Y microspheres. Tech Vasc Interv Radiol 10:12–29
20. Becker C, Waggershauser T, Tiling R, Weckbach S, Johnson T, Meissner O, Klingenbeck-Regn K, Reiser M, Hoffmann RT (2011) C-arm computed tomography compared with positron emission tomography/computed tomography for treatment planning before radioembolization. Cardiovasc Intervent Radiol 34:550–556
21. TheraSphere yttrium-90 glass microspheres [package insert]. Nordion Web site. Available at: http://www.nordion.com/therasphere/physicians-package-insert/package-insert-us.pdf. Accessed July 20, 2013
22. SIR-Spheres microspheres training program: physicians and institutions. Sirtex Web site. Available at: http://www.sirtex.com/files/TRN-US-05.pdf. Accessed October 17, 2012
23. Dezarn WA, Cessna JT, DeWerd LA, Feng W, Gates VL, Halama J, Kennedy AS, Nag S, Sarfaraz M, Sehgal V, Selwyn R, Stabin MG, Thomadsen BR, Williams LE, Salem R, American Association of Physicists in Medicine (2011) Recommendations of the American association of physicists in medicine on dosimetry, imaging, and quality assurance procedures for 90Y microsphere brachytherapy in the treatment of hepatic malignancies. Med Phys 38:4824–4845
24. Rose SC, Hoh CK (2009) Hepatopulmonary shunt reduction using chemoembolization to permit yttrium-90 radioembolization. J Vasc Interv Radiol 20:849–851
25. Bester L, Salem R (2007) Reduction of arteriohepatovenous shunting by temporary balloon occlusion in patients undergoing radioembolization. J Vasc Interv Radiol 18:1310–1314
26. Ahmadzadehfar H, Sabet A, Biermann K, Muckle M, Brockmann H, Kuhl C, Wilhelm K, Biersack HJ, Ezziddin S (2010) The significance of ^{99m}Tc-MAA SPECT/CT liver perfusion imaging in treatment planning for ^{90}Y-microsphere selective internal radiation treatment. J Nucl Med 51:1206–1212
27. Hamami ME, Poeppel TD, Müller S, Heusner T, Bockisch A, Hilgard P, Antoch G (2009) SPECT/CT with ^{99m}Tc-MAA in radioembolization with ^{90}Y microspheres in patients with hepatocellular cancer. J Nucl Med 50:688–692
28. Lenoir L, Edeline J, Rolland Y, Pracht M, Raoul JL, Ardisson V, Bourguet P, Clément B, Boucher E, Garin E (2012) Usefulness and pitfalls of MAA SPECT/CT in identifying digestive extrahepatic uptake when planning liver radioembolization. Eur J Nucl Med Mol Imaging 39:872–880
29. Dudeck O, Wilhelmsen S, Ulrich G, Löwenthal D, Pech M, Amthauer H, Ricke J (2012) Effectiveness of repeat angiographic assessment in patients designated for radioembolization using yttrium-90 microspheres with initial extrahepatic accumulation of technetium-99 m macroaggregated albumin: a single center's experience. Cardiovasc Intervent Radiol 35:1083–1093
30. Kao YH, Tan EH, Teo TK, Ng CE, Goh SW (2011) Imaging discordance between hepatic angiography versus Tc-99m-MAA SPECT/CT: a case series, technical discussion and clinical implications. Ann Nucl Med 25:669–676
31. Ho S, Lau WY, Leung TWT, Chan M, Johnson PJ, Li AKC (1997) Clinical evaluation of the partition model for estimate radiation doses from yttrium-90 microspheres in the treatment of hepatic cancer. Eur J Nucl Med 24:293–298
32. Campbell JM, Wong CO, Muzik O, Marples B, Joiner M, Burmeister J (2009) Early dose response to yttrium-90 microsphere treatment of metastatic liver cancer by a patient-specific method using single photon emission computed tomography and positron emission tomography. Int J Radiat Oncol Biol Phys 74:313–320
33. Flamen P, Vanderlinde B, Delatte P, Ghanem G, Ameye L, Van Den Eynde M, Hendlisz A (2008) Multimodality imaging can predict the metabolic response of un-resectable colorectal liver metastases to radioembolization therapy with yttrium-90 labeled resin microspheres. Phys Med Biol 53:6591–6603
34. Chiesa C, Maccauro M, Romito R, Spreafico C, Pellizzari S, Negri A, Sposito C, Morosi C, Civelli E, Lanocita R, Camerini T, Bampo C, Bhoori S, Seregni E, Marchianò A, Mazzaferro V, Bombardieri E (2011) Need, feasibility and convenience of dosimetric treatment planning in liver selective internal radiation therapy with ^{90}Y microspheres: the experience of the national tumor institute of Milan. Q J Nucl Med Mol Imaging 55:168–197
35. Mazzaferro V, Sposito C, Bhoori S, Romito R, Chiesa C, Morosi C, Maccauro M, Marchianò A, Bongini M, Lanocita R, Civelli E, Bombardieri E, Camerini T, Spreafico C (2013) Yttrium90 radioembolization for intermediate-advanced hepatocarcinoma: a phase II study. Hepatology 57:1826–1837
36. Garin E, Lenoir L, Rolland Y, Edeline J, Mesbah H, Laffont S (2012) Dosimetry based on ^{99m}Tc-macroaggregated albumin SPECT/CT accurately predicts tumor response and survival in hepatocellular carcinoma patients treated with ^{90}Y-loaded glass microspheres: preliminary results. J Nucl Med 53:255–263
37. Garin E, Lenoir L, Edeline J, Laffont S, Mesbah H, Porée P, Sulpice L, Boudjema K, Mesbah M, Guillygomarc'h A, Quehen E, Pracht M, Raoul JL, Clement B, Rolland Y, Boucher E (2013) Boosted selective internal radiation therapy with ^{90}Y-loaded glass microspheres (B-SIRT) for hepatocellular carcinoma patients: a new personalized promising concept. Eur J Nucl Med Mol Imaging 40:1057–1068
38. Sangro B, Gil-Alzugaray B, Rodriguez J, Sola I, Martinez-Cuesta A, Viudez A, Chopitea A, Iñarrairaegui M, Arbizu J, Bilbao JI (2008) Liver disease induced by radioembolization of liver tumors: description and possible risk factors. Cancer 112:1539–1546
39. Chiesa C, Mira M, Maccauro M, Romito R, Spreafico C, Sposito C, Bhoori S, Morosi C, Pellizzari S, Negri A, Civelli E, Lanocita R, Camerini T, Bampo C, Carrara M, Seregni E, Marchianò A, Mazzaferro V, Bombardieri E (2012) A dosimetric treatment planning strategy in radioembolization of hepatocarcinoma with ^{90}Y glass microspheres. Q J Nucl Med Mol Imaging 56:503–508
40. Kao YH, Hock Tan AE, Burgmans MC, Irani FG, Khoo LS, Gong Lo RH, Tay KH, Tan BS, Hoe Chow PK, Eng Ng DC, Whatt Goh AS (2012) Image-guided personalized predictive dosimetry by artery-specific SPECT/CT partition modeling for

safe and effective ^{90}Y radioembolization. J Nucl Med 53:559–566
41. Knesaurek K, Machac J, Muzinic M, DaCosta M, Zhang Z, Heiba S (2010) Quantitative comparison of yttrium-90 (^{90}Y)-microspheres and technetium-99m (^{99m}Tc)-macroaggregated albumin SPECT images for planning ^{90}Y therapy of liver cancer. Technol Cancer Res Treat 9:253–262
42. Jiang M, Fishman A, Nowakowski FS, Heiba S, Zhang Z, Knesaurek K, Weintraub J, Machac J (2012) Segmental perfusion differences on paired Tc-99m macroaggregated albumin (MAA) hepatic perfusion imaging and yttrium-90 (Y-90) bremsstrahlung imaging studies in SIR-sphere radioembolization: association with angiography. J Nucl Med Radiat Ther 3:1
43. Wondergem M, Smits MLJ, Elshot M, deJong HWAM, Verkooijen HM, van den Bosch MA, Nijsen JF, Lam MG (2013) ^{99m}Tc-macroaggregated albumin poorly predicts the intrahepatic distribution of 90Y resin microspheres in hepatic radioembolization. J Nucl Med 54:1294–1301
44. Kao YH, Steinberg JD, Tay YS, Lim GKY, Yan J, Townsend DW et al (2013) Post-radioembolization yttrium-90 PET/CT—part 2: dose-response and tumor predictive dosimetry for resin microspheres. EJNMMI Res 3:57
45. Moore S, Park M, Mueller S (2009) Activity estimation performance in Y-90 microsphere bremsstrahlung SPECT. J Nucl Med 50:1433
46. Walrand S, Hesse M, Demonceau G, Pauwels S, Jamar F (2011) Yttrium-90-labeled microsphere tracking during liver selective internal radiotherapy by bremsstrahlung pinhole SPECT: feasibility study and evaluation in an abdominal phantom. EJNMMI Res 1:32
47. Ahmadzadehfar H, Muckle M, Sabet A, Wilhelm K, Kuhl C, Biermann K, Haslerud T, Biersack HJ, Ezziddin S (2011) The significance of bremsstrahlung SPECT/CT after yttrium-90 radioembolization treatment in the prediction of extrahepatic side effects. Eur J Nucl Med Mol Imaging. [Epub ahead of print]
48. Carlier T, Eugène T, Bodet-Milin C, Garin E, Ansquer C, Rousseau C, Ferrer L, Barbet J, Schoenahl F, Kraeber-Bodéré F (2013) Assessment of acquisition protocols for routine imaging of Y-90 using PET/CT. EJNMMI Res 3:11
49. Elschot M, Vermolen BJ, Lam MG, de Keizer B, van den Bosch MA, de Jong HW (2013) Quantitative comparison of PET and Bremsstrahlung SPECT for imaging the in vivo yttrium-90 microsphere distribution after liver radioembolization. PLoS One 8:e55742
50. Padia SA, Alessio A, Kwan SW, Lewis DH, Vaidya S, Minoshima S (2013) Comparison of positron emission tomography and Bremsstrahlung imaging to detect particle distribution in patients undergoing yttrium-90 radioembolization for large hepatocellular carcinomas or associated portal vein thrombosis. J Vasc Interv Radiol 24:1147–1153
51. Turner JH, Claringbold PG, Klemp PF, Cameron PJ, Martindale AA, Glancy RJ, Norman PE, Hetherington EL, Najdovski L, Lambrecht RM (1994) ^{166}Ho-microsphere liver radiotherapy: a preclinical SPECT dosimetry study in the pig. Nucl Med Commun 15:545–553
52. Nijsen JFW, Seppenwoolde JH, Havenith T, Bos C, Bakker CJG, van het Schip AD (2004) Liver tumors: MR imaging of radioactive holmium microspheres—phantom and rabbit study. Radiology 231:491–499
53. Wong CY, Qing F, Savin M, Campbell J, Gates VL, Sherpa KM, Lewandowski RJ, Nagle C, Salem R (2005) Reduction of metastatic load to liver after intraarterial hepatic yttrium-90 radioembolization as evaluated by [^{18}F]fluorodeoxyglucose positron emission tomographic imaging. J Vasc Interv Radiol 16:1101–1106
54. Bienert M, McCook B, Carr BI, Geller DA, Sheetz M, Tutor C, Amesur N, Avril N (2005) ^{90}Y microsphere treatment of unresectable liver metastases: changes in ^{18}F-FDG uptake and tumour size on PET/CT. Eur J Nucl Med Mol Imaging 32:778–787
55. Szyszko T, Al-Nahhas A, Canelo R, Habib N, Jiao L, Wasan H, Pagou M, Tait P (2007) Assessment of response to treatment of un-resectable liver tumours with ^{90}Y microspheres: value of FDG PET versus computed tomography. Nucl Med Commun 28:15–20
56. Zerizer I, Al-Nahhas A, Towey D, Tait P, Ariff B, Wasan H, Hatice G, Habib N, Barwick T (2012) The role of early ^{18}F-FDG PET/CT in prediction of progression-free survival after ^{90}Y radioembolization: comparison with RECIST and tumour density criteria. Eur J Nucl Med Mol Imaging 39:1391–1399
57. Haug AR, Tiega Donfack BP, Trumm C, Zech CJ, Michl M, Laubender RP, Uebleis C, Bartenstein P, Heinemann V, Hacker M (2012) ^{18}F-FDG PET/CT predicts survival after radioembolization of hepatic metastases from breast cancer. J Nucl Med 53:371–377
58. Haug AR, Heinemann V, Bruns CJ, Hoffmann R, Jakobs T, Bartenstein P, Hacker M (2011) ^{18}F-FDG PET independently predicts survival in patients with cholangiocellular carcinoma treated with 90Y microspheres. Eur J Nucl Med Mol Imaging 38:1037–1045
59. Mumper RJ, Ryo UY, Jay M (1991) Neutron-activated holmium-166-poly (L-lactic acid) microspheres: a potential agent for the internal radiation therapy of hepatic tumors. J Nucl Med 32(11):2139–2143
60. Nijsen JF, van Steenbergen MJ, Kooijman H, Talsma H, Kroon-Batenburg LM, van De Weert M, van Rijk PP, De Witte A, Van Schip AD, Hennink WE (2001) Characterization of poly(L-lactic acid) microspheres loaded with holmium acetylacetonate. Biomaterials 22:3073–3081
61. Nijsen F, Rook D, Brandt C, Meijer R, Dullens H, Zonnenberg B, de Klerk J, van Rijk P, Hennink W, van het Schip F (2001) Targeting of liver tumour in rats by selective delivery of holmium-166 loaded microspheres: a biodistribution study. Eur J Nucl Med 28:743–749
62. Smits ML, Nijsen JF, van den Bosch MA, Lam MG, Vente MA, Mali WP, van Het Schip AD, Zonnenberg BA (2012) Holmium-166 radioembolisation in patients with un-resectable, chemorefractory liver metastases (HEPAR trial): a phase 1, dose-escalation study. Lancet Oncol 13:1025–1034